

# FUV SPECTROSCOPY OF THE DWARF NOVAE SS CYGNI AND WX HYDRI IN QUIESCENCE

KNOX S. LONG

Space Telescope Science Institute, 3700 San Martin Drive, Baltimore, MD 21218

CYNTHIA S. FRONING

Center for Astrophysics and Space Astronomy,  
 University of Colorado, 593 UCB, Boulder, CO, 80309

CHRISTIAN KNIGGE

Department of Physics & Astronomy,  
 University of Southampton,  
 Southampton SO17 1BJ UK

WILLIAM P. BLAIR

Department of Physics and Astronomy, Johns Hopkins University, Baltimore, MD 21218

TIMOTHY R. KALLMAN

NASA/Goddard Space Flight Center, Laboratory for High Energy Astrophysics, Code 662, Greenbelt, MD 20771

AND

YUAN-KUEN KO

Harvard Smithsonian Center for Astrophysics, 60 Garden Street, MS 50, Cambridge, MA 02138

*Draft version June 23, 2018*

## ABSTRACT

We present time-resolved FUV spectra of the dwarf novae SS Cyg and WX Hyi in quiescence from observations using the Hopkins Ultraviolet Telescope on the Astro-1 and Astro-2 Space Shuttle missions and the Goddard High Resolution Spectrograph on the *Hubble Space Telescope*. Both dwarf novae are characterized by blue continua that extend to the Lyman limit punctuated by broad emission lines including transitions of O VI, N V, Si IV, and C IV. The continuum of WX Hyi can be fit with a white dwarf model with physically reasonable model parameters, but neither system actually shows unambiguous signatures of white dwarf emission. The shape and flux of the spectrum of SS Cyg cannot be self-consistently reconciled with a white dwarf providing all of the FUV continuum flux. Combination white dwarf/disk or white dwarf/optically thin plasma models improve the fit but still do not give physically reasonable model parameters for a quiescent dwarf nova. Assuming that the UV emission lines arise from the disk, the line shapes indicate that surface fluxes fall roughly as  $R^{-2}$  in both systems. Fits to the double-peaked line profiles in SS Cyg indicate that the FUV line forming region is concentrated closer to the white dwarf than that of the optical lines and provide no evidence of a hole in the inner disk. Although the flux from SS Cyg was relatively constant during all of our observations, WX Hyi showed significant variability during the GHRS observations. In WX Hyi, the line and continuum fluxes are (with the exception of He II) highly correlated, indicating a link between the formation mechanisms of the line and continuum regions.

*Subject headings:* accretion, accretion disks — binaries: close — novae, cataclysmic variables — stars: individual (SS Cyg) — stars: — individual (WX Hyi) — ultraviolet: stars

## 1. INTRODUCTION

Dwarf novae (DN) are close binary systems in which a main-sequence secondary star loses mass to a non-magnetic white dwarf (WD) via Roche Lobe overflow onto an accretion disk. In the standard accretion theory, the disk radiates away half of the available energy, while

the other half is released in a small boundary layer (BL) between the inner disk and the WD surface. DN undergo quasi-periodic outbursts of 3 – 6 magnitudes due to a thermal instability in the accretion disk that causes a rapid transition from a low-temperature, low-accretion rate state to a high-temperature, high-accretion rate state. During periods of quiescence, the mass transfer rate through the disk is low ( $\leq 10^{15}$  g s<sup>-1</sup>) and the disk is cool ( $T_{\text{disk}} \lesssim 8000$  K) and optically thin in the UV. On the other hand, the BL is likely to be extremely hot ( $T_{\text{BL}} \sim 10^8$  K) and optically thin. As a result, neither the disk nor the BL are expected to produce

Electronic address: long@stsci.edu  
 Electronic address: cfroning@casa.colorado.edu  
 Electronic address: christian@astro.soton.ac.uk  
 Electronic address: wpb@pha.jhu.edu  
 Electronic address: tim@xstar.gsfc.nasa.gov  
 Electronic address: yko@cfa.harvard.edu

large amounts of far-ultraviolet (FUV) flux. Furthermore, since the companion stars are typically K or M dwarfs, they are not significant FUV sources. As a result, the dominant source of FUV emission in quiescent DN is usually assumed to be the WD. Even if the WD were to have cooled in the interval between the common envelope phase and the initiation of mass-exchange, it would have been reheated to temperatures of 10,000 to 50,000 K once mass transfer began (Townesley & Bildsten 2003).

As a result of these expectations, FUV spectra of DN in quiescence have usually been interpreted assuming that the WD dominates, or at least contributes a significant fraction of, the FUV light from the system (Verbunt 1987; Deng et al. 1994). The evidence of WD-dominance is compelling for a few systems, most notably U Gem, VW Hyi, and WZ Sge. In these systems, the WD was first recognized in *IUE* spectra from the broad Ly $\alpha$  absorption and the fact that WD model fits to these spectra yielded temperatures and luminosities that were consistent with the estimated distances to these DN (PANEK & HOLM 1984; MATEO & SZKODY 1984; HOLM 1988). The *IUE* results were then confirmed with higher S/N observations made with the Hopkins Ultraviolet Telescope (HUT), *Hubble Space Telescope* (HST), and the *Far Ultraviolet Spectroscopic Explorer* (FUSE) (Long et al. 1993, 1994a, 2003; Sion et al. 1994, 1995, 2003; Froning et al. 2001; Godon et al. 2004). In these data, the WDs are recognizable not only from the broad Ly $\alpha$  and Ly $\beta$  absorption lines and the overall shape and flux of the UV spectrum, but also from the relatively narrow metal absorption lines, which result from the salting of the atmosphere of the WD by accreting near solar-abundance material.

However, many DN observed in the FUV do not show broad Lyman line absorption features, nor do they show narrow metal absorption lines. Instead, numerous DN (including low inclination systems) show UV spectra characterized by blue continua on which are superposed broad (typically 10 Å FWHM) emission features identifiable with resonance lines such as O VI, N V, Si IV, and C IV. A variety of explanations for the emission lines have been advanced, most involving an optically thin accretion disk (Williams 1980; Tyndal 1981; Menou 2002) or irradiation of the disk by the boundary layer and the WD (Schwarzenberg-Czerny 1981). However, the nature of the continuum emission in quiescent DN has remained controversial. In an attempt to better characterize possible sources of the FUV continuum and line emission in quiescent DN, this article describes FUV observations of two quiescent DN, SS Cyg and WX Hyi, obtained with HUT and with the Goddard High Resolution Spectrograph (GHRS) on *HST*.

SS Cyg is an extremely well-studied U-Gem-type DN, with a period, 6.6 hours, that places it well above the period gap. It is a fairly low ( $\sim 41^\circ$ ) inclination system containing a massive  $1.2 M_\odot$  WD and a  $0.7 M_\odot$  K4 star, which is somewhat overluminous for a main-sequence star of its spectral type (Friend et al. 1990). SS Cyg undergoes outbursts that reach a peak visual magnitude of 8.5, typically lasting either 7 or 15 days and with an average interoutburst period of 50 days (Cannizzo & Mattei 1992; Ak et al. 2002). It is located

at a distance of  $166^{+14}_{-12}$  pc, based on astrometry with the *HST*/FGS (Harrison, et al. 2000). Because it has been observed intensively since its discovery in 1896, SS Cyg has been important as one of the main systems against which detailed predictions of the thermal instability model for DN outbursts have been measured (see, e.g. Cannizzo 1993b). The first UV spectra of SS Cyg were obtained with *IUE* and in quiescence show a ( $F_\lambda$ ) continuum that rises at short wavelengths on which emission lines from a variety of ionization states are superposed (Fabbiano et al. 1981). Some, but not all, quiescent *IUE* spectra show what appears to be a Ly $\alpha$  absorption feature that Holm & Polidan (1988) interpreted as evidence of emission from the WD in the system.

WX Hyi, by contrast, is a SU-UMa-type DN, with a period, 1.8 hours, that places it well below the period gap. It exhibits normal outbursts that last about 1 day every 11.2 days reaching a peak magnitude of 12.7, and superoutbursts lasting about 10 days occurring with a mean interval of 185 days reaching a magnitude of 11.4 (Bateson & McIntosh 1986). The inclination is thought to be comparable to SS Cyg, and the mass of the WD is estimated to be  $0.9 \pm 0.3 M_\odot$  (Schoembs & Vogt 1981), but the secondary has not been detected. The distance to WX Hyi is poorly known, Patterson (1984) estimating 100 pc based on a correlation between H $\beta$  equivalent widths and mass accretion rate, and Warner (1987) estimating 265 pc based on a correlation between period and magnitude during outburst. In quiescence, *IUE* spectra show a flat continuum spectrum, with emission features due to N V, Si IV, C IV and He II (Hassall et al. 1985). There is no indication of absorption near Ly $\alpha$ .

The HUT observations of SS Cyg and WX Hyi in quiescence, which we describe here, provide the first quiescent spectra of these DN that extend the simultaneous wavelength coverage from the Lyman limit to 1840 Å while the GHRS observations provide spectra with far higher S/N and resolution than was available for these objects with *IUE*. The remainder of this paper is organized as follows: The observations and calibration of the data are summarized in § 2. Modeling of the continuum and emission lines is presented in § 3. The results are discussed in § 4, and we present our conclusions in § 5.

## 2. OBSERVATIONS

### 2.1. Hopkins Ultraviolet Telescope

HUT, which flew on the Space Shuttle as part of the Astro-1 and Astro-2 missions in 1990 and 1995, utilized a 0.9 m primary mirror and a prime-focus Rowland circle spectrograph feeding a 1-d photon counting detector to obtain moderate resolution ( $R \sim 3$  Å) spectra of sources covering the wavelength range 820 – 1840 Å (Davidsen et al. 1992; Kruk et al. 1995). SS Cyg was observed once on Astro-1 and on Astro-2 through 18 and 20" diameter circular apertures, respectively. WX Hyi was observed three times on Astro-2 through the 20" aperture. Observation times are listed in Table 1.

On Astro-1, the observation of SS Cyg took place shortly after a "wide"  $\sim 16$  day outburst of the system. The lightcurve obtained by the American Association of Variable Star Observers (AAVSO) indicates that SS Cyg had in fact fallen to its quiescent level of about 12th magnitude, but only within a few days of the observation. It

had been below magnitude 11.5 for about 4 days. The next outburst would not occur for 37 days. In contrast, the Astro-2 observation occurred at the end of a cycle, about 20 days after the previous “narrow” outburst. The next outburst would take place 8 days later.

Because it is relatively faint and in the southern hemisphere, coverage of the light curve of WX Hyi is far less complete than for SS Cyg. However, as a result of a special effort by the AAVSO during the Astro-2 mission, we know that a narrow outburst of WX Hyi took place about 1 day prior to the first HUT observation of WX Hyi, and that WX Hyi remained below magnitude 14, and probably less than magnitude 15, for all three observations of the system. Thus, the observations occurred within a single inter-outburst interval, about 1, 2.5, and 3.1 days after the outburst. Normal outbursts in WX Hyi are typically spaced on 11.2 day intervals (Ak et al. 2002). One AAVSO observer reported WX Hyi in outburst about 12 days after the last HUT observation, which would be roughly consistent with our time line, but there are no confirming observations. A better observed outburst took place about 21 days after the last HUT observation.

For the purposes of this discussion of the HUT observations of SS Cyg and WX Hyi, we have used the final processed data files delivered to the NSSDC, and available through the Multimission Archive at Space Telescope. Unless specifically noted, we have used the photometrically — but not image-motion — corrected data to maximize the counting statistics in the spectra of these relatively faint sources. Most of the observations of SS Cyg and of WX Hyi took place during the daytime portion of the shuttle orbit. However, the Astro-1 observation of SS Cyg contained 814 s of data from orbital night. Since airglow contaminates a significantly greater portion of spectra obtained with HUT during orbital day than during orbital night, nighttime data are preferred when available. Therefore, for the Astro-1 observation of SS Cyg, we have used the 814 s obtained in orbital night in the analysis that follows. Spectra of the Astro-1 and Astro-2 observations of SS Cyg and of the time-averaged (4268 s) Astro-2 spectrum of WX Hyi are shown in Figure 1. The continuum flux levels are close to values reported with *IUE* for SS Cyg and for WX Hyi in quiescence (Fabbiano et al. 1981; LaDous 1990; Hassall et al. 1985).

## 2.2. GHRs

The *HST* observations of SS Cyg and WX Hyi were carried out in the fall of 1996 using the GHRs (Heap et al. 1995). Three observations of each system were made on approximately one month centers using the G140L grating and the LSA aperture (1.74”), yielding a spectral resolution of  $\sim 2000$ . Two grating settings covering the wavelength ranges 1150 – 1435 Å and 1377 – 1663 Å were utilized for each target. For SS Cyg, each 3-orbit observation consisted of two segments, one at each grating setting, which were further divided into individual exposures of 108 s. As a result, twenty spectra at each grating setting were obtained during each of the three observations of SS Cyg. A similar procedure was used for WX Hyi. However, since WX Hyi was observed in *HST*’s continuous viewing zone, each observation was divided into four segments, resulting in forty (108 s integration) spectra at each grating setting.

To ease scheduling (especially for WX Hyi, which has a short inter-outburst period), the observations were not scheduled as targets of opportunity, and as it turned out, two of the observations of each system occurred during an outburst. We will confine ourselves here to the low-state data, obtained on 26 September for SS Cyg and on 5 August for WX Hyi (see Table 1). AAVSO lightcurves indicated that the 26 September observation of SS Cyg occurred in mid-quiescence, about 17 days after return to optical quiescence from a “wide” outburst of SS Cyg, and about 12 days before a “narrow” outburst. The sparse AAVSO data on WX Hyi show that the 5 August observation occurred near the end of a quiescent interval, about 8 days after a normal outburst, and 1 day before another normal outburst.

For the analysis of the *HST* spectra described here, we recalibrated the observations using the standard (CALHRS) pipeline with calibration files available in 1999 February, which properly account for the declining sensitivity of the GHRs at the shortest wavelengths. For wavelength calibration, we elected to register using interstellar lines, although in fact the difference between this and the internal lamp calibration was small ( $< 0.1$  Å). Time-averaged spectra of the low-state GHRs observations are shown in Figure 2.

## 3. ANALYSIS

The FUV spectra of SS Cyg and WX Hyi are characterized by blue continua on which are overlaid strong, broad emission lines from resonance and excited state transitions of ionized metals and He II. SS Cyg also has a broad Ly $\alpha$  absorption feature, which is not seen in WX Hyi. WX Hyi has a richer line spectrum than SS Cyg, with the former showing emission from O VI, N V, and He II, all of which are weak or absent in the latter. The line profiles are double-peaked in SS Cyg, consistent with emission from a Keplerian disk, but are single-peaked in WX Hyi.

There were no dramatic long time scale variations in the shapes of the lines or continuum over the baseline of the HUT observations for either object. The three HUT observations of WX Hyi were obtained during a single quiescent cycle. Between the first and second observations, the continuum declined by 50% but then rebounded in the third observation to a flux midway between the first two (e.g., the 1500 Å continuum fluxes were  $3.3 \times 10^{-14}$ ,  $1.7 \times 10^{-14}$ , and  $2.3 \times 10^{-14}$  ergs cm $^{-2}$  s $^{-1}$  Å $^{-1}$ ). The behavior of the continuum is inconsistent with the report of a steady, long-term decline in the UV line and continuum fluxes given by Hassall et al. (1985). It is also inconsistent with the predictions of the standard disk instability model for DN, which predicts an increase in the disk flux during quiescence (Lasota 2001). In SS Cyg, the continuum level also varied little between the two quiescent observation epochs (spanning a range of six years). The 1500 Å flux was 30% brighter in the first observation and the emission line strengths in Si IV  $\lambda\lambda 1398, 1402$  and C IV  $\lambda 1550$  were  $\sim 60\%$  brighter.

Below, we discuss model fits to the continuum, emission line profiles, and short time scale variability in the FUV spectra of SS Cyg and WX Hyi.

### 3.1. Continuum emission

As noted earlier, the traditional interpretation of FUV continua in quiescent DN has involved emission from WDs with surface temperatures of 10,000 – 50,000 K. For SS Cyg, estimates of the temperature of the WD have ranged from 34,000 – 40,000 K based upon the slope of the continuum and the existence of Ly $\alpha$  absorption in some of the *IUE* spectra (Fabbiano et al. 1981; Holm & Polidan 1988). For WX Hyi, there are no previous estimates of the WD temperature.

In an attempt to see to what degree a WD explanation for the continuum emission in SS Cyg and WX Hyi is viable, we have synthesized sets of  $\log g = 8$  WD model spectra using Hubeny’s TLUSTY and SYNSPEC programs (Hubeny 1988; Hubeny et al. 1994) convolved to the resolution of our HUT and GHRs observations. For comparison, we also synthesized a set of optically-thick steady-state accretion disk spectra from an appropriately weighted set of stellar atmospheres, also constructed with TLUSTY and SYNSPEC, using the procedure described in detail by Long et al. (1994b). In generating the models we have assumed a WD mass of  $1.2 M_{\odot}$  and an inclination of  $41^{\circ}$  for SS Cyg (Friend et al. 1990), while for WX Hyi we have assumed  $0.9 M_{\odot}$  and  $40^{\circ}$  (Schoembs & Vogt 1981). Finally, we have used Cloudy (Ferland 1996) to create a set of model spectra of plasmas in coronal equilibrium. For the thin-plasma spectra we have limited emission to that from H and He since we are here concerned with continuum fits to the data.

We first fit spectra assuming plausible values of the reddening for both SS Cyg and WX Hyi:  $E(B-V) = 0.00, 0.04, \text{ and } 0.07$ . We began with models consisting of either a simple WD, an optically thick accretion disk, or a thin plasma. For WDs, we considered both pure DA atmospheres and atmospheres with a normal heavy element composition. We then considered plausible combinations of WDs and optically thick disks and WDs and thin plasmas. Results of the fits with  $E(B-V)$  set to be 0.04 are recorded in Tables 2 and 3 for SS Cyg and WX Hyi, respectively. All of the fits to the data were carried out using standard  $\chi^2$  minimization techniques. Since the spectra contain emission lines from the disk and (for HUT) from strong airglow lines, we fit only the “line-free” regions of the spectra. Results for the DA model and for the disk fits for the SS Cyg HUT and GHRs data are shown in Figures 3 and 4, while Figures 5 and 6 show the fits to the WX Hyi spectra. Each figure shows the best WD fit and the best disk fit to the data (for SS Cyg, the night-only data from the Astro-1 HUT observations are shown).

For the HUT observation of SS Cyg, the best fitting DA atmosphere (assuming  $E(B-V) = 0.04$ ) is shown in Figure 3. In SS Cyg, the best fit has a temperature of  $\sim 46,000$  K and normalization that corresponds to a WD radius of  $8.2 \times 10^8$  cm at the known distance of  $166^{+14}_{-12}$  pc (Harrison, et al. 2000). The model fit is actually reasonable in a statistical sense ( $\chi^2_{\nu} \sim 1.3$ ) for the fitted regions, but it is important to note that because of the line emission we have excluded most, if not all, of the regions that would contain the strongest signatures of the WD. Best-fitting DA models with  $E(B-V) = 0.0$  and  $0.07$  yield temperatures of 38,000 and 58,000 K, respectively. Increasing  $E(B-V)$  increases the temperature because the model

fits almost entirely reflect the overall slope of the spectrum. The temperature derived from normal-abundance WD models is very similar to that of the DA model.

For the GHRs observation of SS Cyg, the best fitting normal abundance model, again assuming  $E(B-V) = 0.04$ , is shown in Figure 4. The best DA fit has a somewhat lower temperature, 40,800 K, than the HUT model fits and a normalization that corresponds to a WD radius of  $9.7 \times 10^8$  cm. In this case, reflecting the higher statistical quality of the data,  $\chi^2_{\nu} \sim 3$ . The normal abundance model fits provide qualitatively and quantitatively poorer approximations to the GHRs data. By our choice of wavelength ranges to fit, we have actually excluded the strongest absorption lines in the atmosphere of a WD with a temperature of about 37,000 K. Nevertheless, in the high quality data obtained with the GHRs, there are many other lines present in the models that one would expect to observe that are absent in the GHRs spectrum.

If the mass of the WD in SS Cyg is  $1.2 M_{\odot}$ , and if the WD follows a normal WD mass-radius relationship (Panei et al. 2000), then the expected radius of the WD is  $\sim 4.2 \times 10^8$  cm, considerably smaller than the values we have derived. Assuming the lower limit on current estimates of the WD mass in SS Cyg,  $1.0 M_{\odot}$  (Martinez-Pais et al. 1994), gives a maximum WD radius  $\sim 6.3 \times 10^8$  cm, still well below our derived radii. For a WD radius in the range suggested by the mass-radius relationship, the WD temperature (all else remaining equal) would need to be  $\sim 55,000 - 85,000$  K to match the observed continuum flux. However, model WD spectra at these temperatures are too blue in the FUV ( $< 1100$  Å) to match the observed spectra. Thus it is unlikely that the WD dominates the FUV spectrum of SS Cyg.

Disk model fits to the SS Cyg spectra are also shown in Figures 3 and 4. Like the WD models, the disk models approximate the overall slope of the spectrum fairly well and plausibly reproduce the Ly $\alpha$  feature. Despite the fact that the models were constructed with normal abundance atmospheres, the disk models produce no narrow lines because of Doppler broadening. For the HUT and GHRs spectra, the disk models suggest a mass accretion rates of  $1.0 \times 10^{17} \text{ g s}^{-1}$  ( $1.6 \times 10^{-9} M_{\odot} \text{ yr}^{-1}$ ) and  $4.3 \times 10^{16} \text{ g s}^{-1}$  ( $6.8 \times 10^{-10} M_{\odot} \text{ yr}^{-1}$ ), respectively. This is larger than the rates expected from a DN in quiescence. The disk models are normalized to a distance of 100 pc, and so the expected value of the normalization for a distance of 166 pc is 0.36, larger than the best fit normalization would suggest, especially for the higher value of the accretion rate.

Simple thin plasma model fits to the data are poor both for the HUT and GHRs spectra of SS Cyg. This is because simple thin models are not sufficiently blue in the wavelength range longward of 1200 Å, nor do they turn over rapidly enough to match the spectrum in the sub-Ly $\alpha$  range. The best fits tend to the highest temperatures in our grid 100,000 K and have emission measures of order  $3 \times 10^{57} \text{ cm}^{-3}$ .<sup>1</sup> Both combination models, a

<sup>1</sup> We note in passing, that these parameters we derive are not consistent with the expected properties of the BL or corona in quiescent CVs, which in models are much hotter, X-ray sources with  $T \simeq 10^8$  K (Narayan & Popham 1993; Meyer & Meyer-Hofmeister 1994). The problem is not that the temperature is too low since the spectral shape of a thin plasmas does not change significantly in the

WD plus a disk or a WD plus a thin plasma, produce improvements in the model fits to SS Cyg in most cases. In particular, the WD plus thin plasma yields the lowest value of  $\chi^2_\nu \sim 1.1$  for the HUT data and  $\sim 1.4$  for the GHRs. However, the results remain disappointing in the sense that they do not really produce physically believable models for SS Cyg.

The situation for WX Hyi is similar, although there is more variation between the best fits for the HUT and GHRs spectra. For the HUT spectra of WX Hyi, the best fitting DA model WD temperature is 53,800 K and the normalization suggests a radius of  $7.4 \times 10^8$  cm at a fiducial distance of 300 pc. For the GHRs spectrum and normal abundances, the temperature is lower, 25,000 K, and the radius is larger,  $1.9 \times 10^9$  cm. These are plausible values (the M-R relation for a  $0.9 M_\odot$  WD gives a radius  $\sim 7 \times 10^8$  cm), if one assumes that the real signatures of a metal-enriched WD surface have been obscured by the disk emission. As with SS Cyg, however, there are absorption features in regions away from the emission lines that appear in the models but not in the observed spectrum. For disk models and the HUT spectra, the slope of the spectrum requires a mass accretion rate of  $5.1 \times 10^{16} \text{ g s}^{-1}$ . However, if this were actually an accurate description of WX Hyi, then the observed flux should have been an order of magnitude too brighter than observed, assuming a distance of 300 pc. On the other hand, for disk models and the GHRs spectra, one obtains a mass accretion rate of  $3.3 \times 10^{15} \text{ g s}^{-1}$ , and in this case, the flux expected from such a disk is only 25% of that expected if the distance is 300 pc.

So what should one conclude in light of these results? First, while it is true that SS Cyg shows evidence of Ly $\alpha$  absorption and both SS Cyg and WX Hyi have spectral shapes that have the general curvature expected of a WD, it is dangerous to assume the spectrum is actually dominated by the WD; a disk model shows similar features. Second, to make serious progress on interpreting the spectra of DN in quiescence it is going to be necessary to develop better models of other components in the system. We will return to this topic in § 4.

### 3.2. Time-averaged emission spectra

#### 3.2.1. Modeling the emission line profiles

If we assume that the emission lines observed in SS Cyg and WX Hyi are produced on a surface layer of the disk, then the shape of the emission lines constrain the region of the disk where the emission lines originate. This is because, in a geometrically thin, flat accretion disk in Keplerian rotation, Doppler broadening dominates the line broadening for optically thin lines. By assuming a local line surface brightness profile, such as  $f(R) \propto R^{-\alpha}$ , and summing over the contribution of the entire disk, a model emission line profile can be made that depends on the radial extent of the line-forming region (or alternatively, the ratio of the inner to outer disk radii), the velocity at the disk edge, and the value of the power law

index,  $\alpha$  (Smak 1981). Such models produce the classic double-peaked emission line profiles characteristic of accretion disks in Keplerian rotation. In these models,  $\alpha$  sets the shape of the line wings, the radial extent of the disk controls the extent of the line wings, and the velocity at the disk edge determines the separation of the line peaks. For optically thick emission lines, shear broadening becomes important, and the line profiles depend additionally on inclination (Horne & Marsh 1986; Orosz et al. 1994). Including shear for optically thick lines has the primary effect of deepening the central minimum between the line peaks at moderate to high binary inclinations.

Following the formalism of Orosz et al. (1994), we modeled the line profiles of the strong UV emission lines in the averaged GHRs spectra of SS Cyg and WX Hyi. The doublet nature of most of the lines and the finite instrument resolution were taken into account in the fits. In Figures 7 and 8 we compare the shapes of the emission lines to the best-fitting theoretical line profiles for both the optically thin and optically thick cases. The corresponding model output parameters are given in Table 4. For SS Cyg, the optically thin line profiles provide better fits to the observed emission lines. The deepening of the central depression between the line peaks for the optically thick models is a small but appreciable effect at the moderate inclination of SS Cyg and worsens the fit to the lines. The primary evidence for optically thin UV line emission in SS Cyg comes from the doublet ratios of the Si IV and C IV lines, where the model fits are clearly better for a ratio of 2:1 (optically thin) than 1:1 (optically thick). The opposite result holds true for WX Hyi, in which the optically thick models are more consistent with the observed line shapes than the optically thin ones. This conclusion is based on how the models fit the doublet line ratios rather than how they fit the depths of the line centers relative to the peaks, since in WX Hyi the observed line profiles are not double-peaked. For both SS Cyg and WX Hyi, the power law index,  $\alpha$ , varies from 1.8 – 2.5 for the different emission lines (with a few large excursions from this range, such as the optically thick model of N V in WX Hyi). The value of  $\alpha$  controls the shape of the line wings in the models, and it is clear from Figures 7 and 8 that our models are not always descriptive of the observed line wings. In general, however, the surface brightness varies roughly as  $f(R) \propto R^{-2}$  for the UV emission lines in SS Cyg and WX Hyi, which is consistent with the surface brightness distributions of optical emission lines in CVs (see Robinson et al. 1993, and sources therein).

In SS Cyg, the observed emission lines are double-peaked. For a Keplerian accretion disk, the velocity separation between the peaks corresponds to twice  $V_K \sin i$  at the outer radius of the line formation region, giving a lower limit to the size of the disk. The best-fit optically thin line profile models for SS Cyg give  $V_K \sin i$  equal to  $490^{+75}_{-33}$ ,  $470^{+52}_{-44}$ , and  $280^{+19}_{-60} \text{ km s}^{-1}$  for C II, Si IV, and C IV, respectively. For the Balmer series, Martinez-Pais et al. (1994) give  $V_K \sin i = 178, 245, 294$ , and  $307 \text{ km s}^{-1}$  for H $\alpha$  to H $\delta$ . If all of the emission lines originate in a fully Keplerian accretion disk, the velocity separations of the UV line peaks in SS Cyg indicate that their line formation regions cut off at smaller radii (higher disk velocity) than those of the optical emission

FUV at temperatures higher than 100,000 K. Rather, the problem is that if the temperature were  $10^8 \text{ K}$ , then the required emission measure would be of order  $10^{59} \text{ cm}^{-3}$ , as compared to estimates, in the case of SS Cyg, of  $2 \times 10^{56} \text{ cm}^{-3}$  (Done & Osborne 1997). To connect this plasma to the BL or high T corona, one would need to invoke a more complicated models with a much tighter connection to a physical picture of the source of the emission.

lines. The strongest UV line, C IV, does extend to outer disk radii comparable to those of the Balmer emission lines above H $\alpha$ .

### 3.2.2. Searching for a hole in the inner accretion disk

Although DN outbursts are in most respects well described by the thermal-viscous disk instability model (see, e.g., Cannizzo 1993a, for a review), the standard model is unable to account for the 0.5–1 d delay between the start of outbursts at optical and UV wavelengths observed in several DN (e.g., Hassall et al. 1983; Polidan & Holberg 1984; Verbunt 1987). A number of theoretical models have attempted to explain the optical–UV lag by arguing that the inner accretion disk is disrupted during the inter-outburst interval and must be replenished before the UV outburst can begin. Mechanisms for disrupting the inner disk include a coronal siphon (Meyer & Meyer-Hofmeister 1994), a weak WD magnetic field (Livio & Pringle 1992), or irradiation by the hot WD (King 1997). Typical models predict that the inner radius of the accretion disk moves out to  $R_{inner} \sim 3 - 4.5 \times 10^9$  cm far from outburst (Liu et al. 1997; King 1997).

Such a hole in the accretion disk should be observable in high excitation emission lines (i.e., those we most expect to be associated with the inner disk), and would be reflected in a loss of the high-velocity line wings. We undertook to determine the inner radii of the UV line emitting regions in SS Cyg (for which the double-peaked emission lines strongly support an accretion disk origin). Assuming Keplerian disk rotation, the inner radius of the line formation region is related to the observed maximum velocity of the emission line (or the HWZI) by

$$v_{max} = \sqrt{\frac{GM_{WD}}{R_{inner}}} \sin i \quad (1)$$

where we set  $M_{WD} = 1.2 M_{\odot}$  and  $i = 41^{\circ}$ . We determined  $v_{max}$  from the model fits to the normalized emission line profiles (Table 4). We used the optically thin models for SS Cyg, although the resulting values of  $R_{inner}$  do not depend on details of the model fitting but only on a correct measure of the maximum velocity in the line wings. We found  $R_{inner} = 1.7^{+0.3}_{-1.4} \times 10^9$ ,  $1.3^{+0.7}_{-0.8} \times 10^9$ , and  $2.4^{+2.4}_{-1.0} \times 10^9$  cm for the C II, Si IV, and C IV emitting regions. As a check, we also directly estimated the HWZI of the emission lines using Gaussian fits to the doublets; our results were consistent with those quoted above to within the error bars.

Thus, the inner radii of the UV emission line formation regions are 2 to 4 times smaller than the size of the hole in the disk predicted by theoretical models. If the UV emission lines in SS Cyg originate in a Keplerian accretion disk, there is no evidence for substantial disruption in the inner accretion disk in quiescence. The complex emission line profiles observed in SS Cyg and the lack of double-peaked profiles in WX Hyi and other CVs underscores that our current emission line models are incomplete, however; sub-Keplerian rotation and/or the presence of vertically extended line emission could still allow for a hole in the inner accretion disk during quiescence.

### 3.3. Variability in the emission lines and the continuum

As noted earlier, the GHRS observations comprise a series of spectra with individual integration times of 108 s. Given that the spectra are individually of high S/N, we investigated whether the spectra exhibit variations on this time scale, since time variations might provide clues to the nature of the emitting regions in the lines or the continuum, or both.

From our initial inspection of the data, it was clear that there were large difference in the individual spectra of WX Hyi, but that, to first order, SS Cyg was not varying. To begin to characterize the variability, or lack thereof, in the two datasets, we first computed the fractional variance spectrum,

$$\sigma^2(\lambda) = \frac{1}{N-1} \sum_{n=1, N} \left( \frac{f_n(\lambda)}{\langle f(\lambda) \rangle} - 1 \right)^2 \quad (2)$$

where  $N$  is the total number of spectra,  $f_n(\lambda)$  is the observed flux in the  $n^{th}$  spectrum, and  $\langle f(\lambda) \rangle$  is the flux in the mean spectrum. We have then compared this to the variance expected due to counting statistics, i.e.,

$$\sigma_{stat}^2(\lambda) = \frac{1}{N} \sum_{n=1, N} \left( \frac{E(f_n(\lambda))}{\langle f(\lambda) \rangle} \right)^2 \quad (3)$$

where  $E(f_n(\lambda))$  is the uncertainty in the  $n^{th}$  spectrum. Results of this evaluation are presented in Figure 9, which shows the fractional variance spectrum of each object normalized with respect to the expected statistical variance. The solid and dashed lines indicate, respectively, the expectation value and the value at which there is a 1% probability of a single point exceeding that level for no intrinsic variability (Knigge et al. 1997).

This analysis confirmed the impressions obtained from our inspection of the individual spectra. For SS Cyg, there is no evidence of variability in the continuum; the ratio of the fractional variance to the variance expected from counting statistics is close to 1 at all wavelengths. Several of the emission lines show low-level variability. The strongest non-statistical variation is seen in Ly $\alpha$ , but this feature is contaminated by terrestrial airglow. C IV shows the strongest variability of the non-contaminated emission lines. Examination of fluxes in the individual spectra places the 1- $\sigma$  continuum variability at <4%, while the peak C IV line flux has a maximum deviation from the mean flux of 12%.

In WX Hyi, on the other hand, both the continuum and the emission lines show variability in excess of purely statistical variation at all wavelengths. Examination of spectra shows that variations occurred on time scales at least as short as individual exposures. The strongest source variation is seen in N V. In order to determine the extent to which the emission line and continuum variations are correlated in WX Hyi, we fit the strong emission lines and the underlying continua in the individual spectra of each system using SPECFIT (Kriss 1994). We fit each line locally with a flat continuum and a Gaussian emission profile. We modeled the doublet lines with two Gaussians with equal FWHM and the relative positions of the doublet transitions fixed. The other emission features were modeled as single lines. We verified that the Gaussian fits agreed to within the uncertainties determined by SPECFIT to a direct calculation of the line

EW obtained by summing over the line. Deviations between the two methods almost always depended on the placement of the continuum level, which the statistical fit of SPECFIT is best equipped to determine.

Plots of emission line fluxes and equivalent widths versus continuum fluxes in WX Hyi are shown in Figures 10 and 11. All of the emission lines except for He II increase in line flux with increased continuum level. The continuum flux showed both short-term flickering on the time scale of the individual spectra as well as a more general rise in continuum level over the full observation. The correlation between the line and continuum fluxes is fairly tight for all of the lines, suggesting that the line fluxes track the continuum for both the rapid flickering and the broad continuum rise. There is no lag between changes in the continuum and line fluxes, although our 108 s integrations are not sensitive to shorter time scales on which such lags might be expected to occur.

In N V, Si III  $\lambda$ 1298, C III, and C II, the EW remains roughly constant with the continuum level. The constant EWs and increasing line fluxes in these lines indicate that their line fluxes increase equally with the continuum flux. In C IV, Si IV, and He II, the EW of the line decreases as the continuum rises. In C IV and Si IV, the decline in EW is coupled with an increase in the line flux, indicating that the lines respond to or with the continuum but are not directly proportional to the continuum flux level. This behavior, which has also been observed in Wolf-Rayet star winds (Morris, Conti, Lamers, & Koenigsberger 1993), is known as the Baldwin (1977) effect when observed in quasars. The decreasing EWs in C IV and Si IV suggest that these two lines are nearly saturated. Alternately, it could indicate a change in the ionization state of the line formation region. N V may have a higher ion abundance than C IV and Si IV and is therefore not near saturation, or changes in the ionization balance with increasing flux may increase the N V ion population relative to the other two ions. The He II measurements show more scatter than for the other lines. There is no sign of a correlated change in the line flux with continuum, suggesting that the He II emission is decoupled from the local FUV continuum emission.

Finally, we searched for evidence of systematic changes in the profiles of the emission lines as the continuum and line fluxes varied. The Gaussian fits to the emission lines showed no trend in the line width (Gaussian FWHM) with continuum or line flux level. We also examined smoothed averages of the five spectra with the lowest continuum levels and the five with the highest continua in each grating setting. There was no indication of a systematic difference between the emission line shapes and no appreciable change in the shape of the continuum between the “low” and “high” averaged spectra. The constancy of the continuum and the emission line shapes as the flux levels increase suggests that the variability occurs throughout the UV emission line formation region.

#### 4. DISCUSSION

##### 4.1. The continuum source

The primary motivation of this study was to better constrain the sources of FUV emission in quiescent DN. In this respect, the continuum modeling results have been

disappointing. WD models provide a reasonable fit to the shape of the continuum in WX Hyi with realistic parameter values, but there are no actual signatures of a WD in the spectrum. The GHRS spectrum is of high resolution and S/N, but the narrow absorption features present in the model WD spectrum are not seen in the observed spectrum. Most of the absorption transitions are coincident with the strong emission features and could be masked, but this is not true of all: e.g., at 1280 Å (see Figure 6). It is also difficult to reconcile the prominent WD absorption lines at C III  $\lambda$ 1176 and Si II  $\lambda$ 1262 and  $\lambda$ 1529 with the lack of absorption dips at zero velocity in the relatively weak emission profiles. Furthermore, for WX Hyi, it would be very difficult to interpret the coordinated line and continuum variations that are observed in the GHRS spectra in terms of a photospheric emission from the WD.

In the case of SS Cyg, there are some reasons for believing that the WD should be fairly hot assuming its current behavior is typical of the long-term average behavior. Indeed, Schreiber & Gänsicke (2002) have argued that an implication of the *HST*/FGS parallax of SS Cyg is that the time averaged accretion rate needs to be of order  $4.2 \times 10^{17} \text{ g s}^{-1}$ , a rate that is normally measured for nova-likes and/or the Z Cam systems. A combination of compressional heating (the readjustment of the interior structure of the WD to accreted material) and nuclear burning of accreted material would cause the photospheric temperature of such a system to rise to 40,000–60,000 K (Townsend & Bildsten 2003) if this is the long-term average accretion rate. Several Z Cam and related systems, including MV Lyr (Hoard et al. 2004), DW UMa (Araujo-Betancor et al. 2003) and Z Cam (Hartley et al. 2005) itself do have measured WD temperatures in this range.

However, as we have pointed out, to match the observed flux, model WD spectra that fit the shape of the continuum are about 2 times larger in WD radius than the value indicated by WD mass-radius relationships. Another way of saying this is that a WD with the expected radius at the known distance can only supply 25% of the flux at the distance. Clearly, this result depends upon an accurate distance to SS Cyg, but the distance ( $166^{+14}_{-12}$  pc) should be reliable, given that it is based upon *HST*/FGS astrometry (Harrison, et al. 2000). A lower WD mass would also help to reconcile the difference, but a WD mass of  $0.68 M_{\odot}$  seems unreasonable based on the existing optical studies (Friend et al. 1990). Hotter WDs can match the flux but are too blue at short wavelengths to fit the spectral shape. (To maximize the contribution from the WD, one would look for a second source with a lower color temperature than the WD.) As with WX Hyi, there are no unambiguous signatures of the WD in the FUV spectrum. SS Cyg has a broad Ly $\alpha$  absorption feature, but accretion disk model fits show that Doppler-broadened absorption in (a portion of) the disk can, in principle, explain this feature. Again, the narrow absorption lines that appear in the normal abundance WD models are not seen in the high S/N GHRS spectrum.

Therefore, it is evident for both SS Cyg and for WX Hyi that another continuum source contributes substantially to the FUV spectrum. This is not unique to

the emission line systems: even in quiescent DN for which the WD dominates the FUV spectrum there is evidence of another continuum source in the FUV. VW Hyi shows a flux excess near the Lyman limit and variability, neither of which are attributable to the WD (Godon et al. 2004). For U Gem, in some sense the prototypical WD-dominated DN, WD model fits are improved when a second temperature component is added — and the second component is required in U Gem to reconcile flux and temperature changes in the FUV spectrum during quiescence (Long et al. 1995). Additional absorbing material along the line of sight to the WD is also evident in U Gem and WZ Sge from the presence of transitions of S VI, O VI, N V, and Si IV that are not produced in their WDs and from the improvement in model fits when an absorbing slab is placed between the WD and the observer (Froning et al. 2001; Long et al. 2003).

The second source in the FUV has been variously attributed to an “accretion belt” on the surface of the WD, disk emission resulting from ongoing accretion during quiescence, or a disk corona (Long et al. 1993; Meyer & Meyer-Hofmeister 1994). What is lacking for all of these models are detailed calculations of expected parameter values to compare to the observations. The structure and physical conditions of quiescent accretion disks remain poorly understood, limiting our ability to select between competing models. Our combined model fits to SS Cyg showed that steady-state accretion disk and simple optically thin plasma models could not provide good fits with realistic parameter values (mass accretion rates, temperatures, and fluxes). The accretion disk model results are not surprising. Both observations and the predictions of the disk instability model argue that quiescent disks are not in a steady state (Lasota 2001; Horne 1993). Plasma models are promising but unconstrained, with the simple, single-temperatures models we used unable to fit the shape of the spectrum. Chandra observations of WX Hyi show that the X-ray spectrum arises from a dense, multi-temperature plasma, with temperatures from  $10^6$  to  $\geq 10^8$  K and densities of  $n \sim 10^{13} - 10^{14} \text{ cm}^{-3}$  (Perna et al. 2003). Comparison of the X-ray spectrum to standard models for quiescent DN (BL, coronas, cooling flows) show that these models underpredict the cool gas component and the long wavelength emission, suggesting that an intermediate-temperature component to the quiescent emission remains unexplored.

#### 4.2. The UV line emission

The strong emission line spectra seen in WX Hyi and SS Cyg can be compared to models of emission line formation in quiescent DN. Ko et al. (1996) made detailed, non-LTE calculations of the vertical structure and emergent spectrum of a temperature-inverted layer overlying the accretion disk in quiescent DN. In their model, a line-emitting accretion disk chromosphere is created by photoionization of the disk by an external X-ray/EUV source. In order to generate UV line fluxes comparable to those observed in quiescent DN, their model requires a large illuminating factor of the disk ( $\sim 0.1$ ) and illuminating X-ray luminosities that are as large at the outer disk radii as at the inner radii. In addition, they find that observed hard X-ray luminosities in DN are too low to generate observed line fluxes using their model, and they postulate the existence of an additional EUV/soft

X-ray component with  $L_X \gtrsim 10^{32} \text{ ergs s}^{-1}$ .

In Table 4, we compare our observed emission line flux ratios and radial surface brightness indices with those of the two-component models of Ko et al. In their two-component models, the hard X-ray component is fixed while the luminosity and shape of the soft X-ray/EUV component is varied. Given that the models are not tailored to apply to specific DN, there is actually fairly good agreement between the line flux ratios we observed in SS Cyg and WX Hyi and those predicted by the models. The line ratios in SS Cyg correspond most closely with their Case 9, which uses a 5 keV Bremsstrahlung with  $L_X = 9 \times 10^{29} \text{ ergs s}^{-1}$  and a 0.1 keV Bremsstrahlung with  $L_X = 1 \times 10^{32} \text{ ergs s}^{-1}$  for the two-component X-ray photoionizing source. The line ratios in WX Hyi are closer to Case 8, which has a stronger soft X-ray component,  $L_X = 1 \times 10^{33} \text{ ergs s}^{-1}$ .

The photoionization models have some deviations from the observations, though. The models do not predict the low N V / C II ratio observed in SS Cyg, but N V is surprisingly weak in SS Cyg compared to other DN (Mauche et al. 1997). A more serious discrepancy is the ratio of He II to the resonance lines: the models that most closely match the observed UV resonance line ratios in SS Cyg and WX Hyi vastly over-predict the He II / C IV ratio. This is a general problem with photoionization models: the flux in the He II recombination line depends directly on the strength of the ionizing soft X-ray/EUV component and when the luminosity of the soft component is increased to match the observed resonance line fluxes, the He II line is over-produced. A comparison of the radial surface brightness indices based on our fits to the emission line profiles and those of the models also suggests that the observed UV line surface brightnesses drop off more rapidly with disk radius than predicted by the models. The Ko et al. (1996) models are strictly generic, however, so models that take into account the individual system parameters of SS Cyg and WX Hyi could resolve this discrepancy.

The variability properties of the spectrum in WX Hyi also constrain the source of the FUV emission lines. All of the strong emission lines, except for He II, follow the variability in the continuum with no lag on 108 sec time scales. While most of the lines remain constant in EW as the continuum rises, the Si IV and C IV lines decrease in EW. These lines may be at or nearing saturation, although it is also possible that the ionization structure of the line-emitting region changes as the continuum flux increases, causing Si and C to be ionized out of these levels. In any event, all of the resonance lines track the FUV continuum, indicating that the two regions and formation mechanisms are linked. The recombination line of He II does not vary with the other lines and the FUV continuum in WX Hyi, suggesting that variations in the soft X-ray/EUV component are not the source of the flickering. Ko et al. (1996) note that disk photospheric radiation is an important photoionization source for line formation in DN, especially at small disk radii. The radial surface brightness profiles for both DN are steeper than the model predictions, indicating that the observed lines are more centrally concentrated than in the models. Photoionization by the disk may therefore be more significant than irradiation from the central X-ray source for the formation of the lines in these DN, a conclusion



that is consistent with the correlation of the FUV disk and line flux variability.

### 5. CONCLUSIONS

In this report, we have analyzed FUV spectra of SS Cyg and WX Hyi, as observed with HUT and the GHRS. The HUT spectra in particular are the first spectra to have been obtained of these objects in quiescence that extend to the Lyman limit. Our results can be summarized as follows:

1. The quiescent FUV spectra of WX Hyi and SS Cyg are characterized by blue continua and strong, broad emission lines from ionized species including O VI, N V, C IV, Si IV, He II, and C III. The HUT spectra of WX Hyi, obtained during a single interoutburst interval, show no sign of a steady increase or decrease in FUV flux during quiescence.
2. Model fits to the continuum using WD, steady-state accretion disk, an optically thin plasma, and combined fits show that both WD and disk models can fit the continuum shapes in SS Cyg and WX Hyi. However, the narrow absorption features expected from a WD are not seen in the spectra, although the strongest transitions are masked by line emission. Furthermore, at the known distance to SS Cyg, the pure WD model fits require WD radii in excess of that expected from WD mass-radius relations. None of the continuum models provide fits with realistic parameters.
3. The line profiles in SS Cyg are double-peaked with doublet ratios that indicate optically thin lines, while the line profiles in WX Hyi are single-peaked with optically thick doublet ratios. Model fits to the line profiles give radial surface brightness distributions of  $f(R) \propto R^{-2}$  for the FUV lines in both systems. For SS Cyg, the half-separation between the emission line peaks is larger for the UV lines than for the optical Balmer lines, indicating that the UV line formation regions is more centrally concentrated. Based on the velocity extent of the emission line wings in SS Cyg, there is no evidence for a hole in the center of the accretion disk.
4. The spectra of SS Cyg showed little variability during the observations. The GHRS spectra of WX Hyi, on the other hand, are highly variable in both lines and continuum on the time scale (108 sec) of the individual spectra. There was no observed lag between the continuum and line variations. All of the strong lines except He II increased

in flux as the continuum increased. He II showed no coordinated response to continuum variations. In C IV and Si IV, the EW dropped with increasing continuum flux, providing the first examples of which we are aware of a so-called Baldwin effect for DN, while for the other lines the EW stayed constant. C IV and Si IV may be near saturation, or the ionization state of UV emitting gas changes as the continuum flux increases. The emission line profiles and the shape of the continuum did not change over the observations. Since the lines presumably arise in the disk, the coordinated variability of the lines and continuum in WX Hyi provides another indication of the strength of a “second” component in the spectrum.

5. The UV behavior of both WX Hyi and SS Cyg are qualitatively in agreement with the predictions of photoionized emission line formation models but discrepancies — such as the weakness of observed He II recombination emission relative to the model predictions — between the observations and the models remain.

SS Cyg (especially) and WX Hyi are well-studied DN. Our investigation of FUV spectra highlights our the current lack of quantitative understanding of the physical conditions that give rise to the FUV spectra of these two DN in quiescence. Although most observers (including ourselves) have tended to concentrate on simpler WD-dominated systems in quiescence, SS Cyg and WX Hyi are not unique. Many other quiescent DNe are wholly dominated by or have significant contributions from a “second” component, most probably the same component that is so prominent in SS Cyg and WX Hyi. The exploratory work of Ko et al. (1996) aside, there have been few attempts to change the situation regarding modeling of quiescent DN (in part because the technical challenges remain significant). However, in the absence of such modeling, it is hard to assert we have a good understanding of the physics of DN, and which of several possible mechanisms give rise to the FUV emission that is observed. More of us need to undertake the challenge implied by spectra of the type observed here.

We acknowledge with thanks the variable star observations from the AAVSO International Database contributed by observers worldwide and used in this research. This work was supported by NASA through grant G0-6544 from the Space Telescope Science Institute, which is operated by AURA, Inc., under NASA contract NAS5-26555.

### REFERENCES

- Ak, T., Ozkan, M. T., & Mattei, J. A. 2002, *A&A*, 389, 478  
Araujo-Betancor, S., et al. 2003, *ApJ*, 583, 437  
Baldwin, J. A. 1977, *ApJ*, 214, 679  
Bateson, F. M., & McIntosh, R. 1986, *Royal Astronomical Society of New Zealand Publications of Variable Star Section*, 14, 1  
Cannizzo, J. K., & Mattei, J. A. 1992, *ApJ*, 401, 642  
Cannizzo, J. K., 1993a, in *Accretion Discs in Compact Stellar Systems*, ed. J. C. Wheeler (Singapore: World Scientific Publishing), 6  
Cannizzo, J. K. 1993b, *ApJ*, 419, 318  
Davidsen, A. F., et al. 1992, *ApJ*, 392, 264  
Deng, S., Zhang, Z., & Chen, J. 1994, *A&A*, 281, 759  
Done, C., & Osborne, J. P. 1997, *MNRAS*, 288, 649  
Fabbiano, G., Hartmann, L., Raymond, J., Branduardi-Raymont, G., Matilsky, T. & Steiner, J. 1981, *ApJ*, 243, 911  
Ferland, G. J. 1996, *Hazy, a Brief Introduction to Cloudy*, Univ. of Kentucky Dept. of Phys. and Astron. Internal Report  
Friend, M. T., Martin, J. S., Connon-Smith, R., & Jones, D. H. P. 1990, *MNRAS*, 246, 637  
Froning, C. S., Long, K. S., Drew, J. E., Knigge, C., & Proga, D. 2001, *ApJ*, 562, 963

- Godon, P., Sion, E. M., Cheng, F. H., Szkody, P., Long, K. S., & Froning, C. S. 2004, *ApJ*, 612, 429
- Harrison, T. E., McNamara, B. J., Szkody, P., & Gilliland, R. L. 2000, *AJ*, 120, 2649
- Hartley, L. E., Long, K. S., Froning, C. S., & Drew, J. E. 2005, *ApJ*, in press
- Hassall, B. J. M., Pringle, J. E., & Verbunt, F. 1985, *MNRAS*, 216, 353
- Hassall, B. J. M., Pringle, J. E., Schwarzenberg-Czerny, A., Wade, R. A., Whelan, J. A. J. & Hill, P. W. 1983, *MNRAS*, 203, 865
- Heap, S. R., et al. 1995, *PASP*, 107, 871
- Hoard, D. W., Linnell, A. P., Szkody, P., Fried, R. E., Sion, E. M., Hubeny, I., & Wolfe, M. A. 2004, *ApJ*, 604, 346
- Holm, A. V., & Polidan, R. S. 1988, in *ESA SP-281 A Decade of UV Astronomy with the IUE Satellite*, ed by E. J. Rolf, (ESTEC, Paris), Volume 1, 179
- Holm, A. V. 1988, in *ESA SP-281 A Decade of UV Astronomy with the IUE Satellite*, ed. by E. J. Rolf, (ESTEC, Paris) Volume 1, 229
- Horne, K. 1993, in *Accretion Disks in Compact Stellar Systems*, Vol. 9, *Advanced Series in Astrophysics and Cosmology*, ed. J. C. Wheeler (Singapore: World Scientific Publishing Co. Pte. Ltd.), 117
- Horne, K., & Marsh, T. R. 1986, *MNRAS*, 218, 761
- Horne, K., & Steining, R. F. 1985, *MNRAS*, 216, 933
- Hubeny, I. 1988, *Comput. Phys. Comm.*, 52, 103
- Hubeny, I., Lanz, T., & Jeffery, C. S. 1994, *Newsletter on Analysis of Astronomical Spectra* (St. Andrews: St. Andrews Univ.), 20, 30
- King A. R. 1997, *MNRAS*, 288, L16
- Knigge, C., Long, K. S., Blair, W. P., & Wade, R. A. 1997, *ApJ*, 476, 291
- Ko, Y. -K., Lee, Y. P. , Schlegel, E. M. Kallman, T. R. 1996, *ApJ*, 457, 363
- Kriss, G. 1994, *Astronomical Society of the Pacific Conference Series*, 61, 437
- Kruk, J. W., Durrance, S. T., Kriss, G. A., Davidsen, A. F., Blair, W. P., Espey, B. R. Finley, D. S. 1995, *ApJ*, 454, L1
- LaDous, C. 1990, *Space Sci. Rev.*, 52, 203
- Lasota, J.-P. 2001, *New Astronomy Review*, 45, 449
- Liu, B. F., Meyer, F., & Meyer-Hofmeister, E. 1997, *A&A*, 328, 247
- Livio, M., & Pringle, J. E. 1992, *MNRAS*, 259, 23P
- Long, K. S., Froning, C. S., Gänsicke, B., Knigge, C., Sion, E. M., & Szkody, P. 2003, *ApJ*, 591, 1172
- Long, K. S., Blair, W. P., & Raymond, J. C. 1995, *ApJ*, 454, L39
- Long, K. S., Wade, R. A., Blair, W. P., Davidsen, A. F. & Hubeny, I. 1994, *ApJ*, 426, 704
- Long, K. S., Sion, E. M., Huang, M. & Szkody, P. 1994, *ApJ*, 424, L49
- Long, K. S., Blair, W. P., Bowers, C. W., Davidsen, A. F., Kriss, G. A., Sion, E. M. & Hubeny, I. 1993, *ApJ*, 405, 327
- Martinez-Pais, I. G., Giovannelli, F., Rossi, C. & Gaudenzi, S. 1994, *A&A*, 291, 455
- Mateo, M. & Szkody, P. 1984, *AJ*, 89, 863
- Mauche, C. W., Lee, Y. P., & Kallman, T. R. 1997, *ApJ*, 477, 832
- Menou, K. 2002, in *The Physics of Cataclysmic Variables and Related Objects*, eds. B. T. Gänsicke, K. Beuermann, & K. Reinsch, *ASP Conf. Ser.*, 261, 387
- Meyer, F., & Meyer-Hofmeister, E. 1994, *A&A*, 288, 175
- Morris, P., Conti, P. S., Lamers, H. J. G. L. M., & Koenigsberger, G. 1993, *ApJ*, 414, L25
- Narayan, R., & Popham, R. 1993, *Nature*, 362, 820
- Orosz, J. A., Bailyn, C. D., Remillard, R. A., McClintock, J. E., & Foltz, C. B. 1994, *ApJ*, 436, 848
- Panei, J. A., Althaus, L. G., & Benvenuto, O. G. 2000, *A&A*, 353, 970
- Panek, R. J., & Holm, A. V. 1984, *ApJ*, 277, 700
- Patterson, J. 1984, *ApJS*, 54, 443
- Perna, R., McDowell, J., Menou, K., Raymond, J., & Medvedev, M. V. 2003, *ApJ*, 598, 545
- Polidan, R. S. & Holberg, J. B. 1984, *Nature*, 309, 528
- Robinson, E. L., Marsh, T. R. & Smak, J. I. in *Accretion Disks in Compact Stellar Systems*, ed. J. C. Wheeler (Singapore: World Sci. Pub. Co. Pte. Ltd.), 75
- Schoembs, R., & Vogt, N. 1981, *A&A*, 97, 185
- Schreiber, M. R., & Gänsicke, B. T. 2002, *A&A*, 382, 124
- Schwarzenberg-Czerny, A. 1981, *Acta Astronomica*, 31, 241
- Sion, E. M., et al. 2003, *ApJ*, 592, 1137
- Sion, E. M., Huang, M. , Szkody, P. & Cheng, F. 1995, *ApJ*, 445, L31
- Sion, E. M., Long, K. S., Szkody, P., & Huang, M. 1994, *ApJ*, 430, L53
- Smak, J. 1981, *Acta Astronomica*, 31, 395
- Townsley, D. M., & Bildsten, L. 2003, *ApJ*, 596, L227
- Tylenda, R. 1981, *Acta Astronomica*, 31, 127
- Verbunt, F. 1987, *A&A*, 71, 339
- Warner, B. 1987, *MNRAS*, 227, 23
- Williams, R. E. 1980, *ApJ*, 235, 939

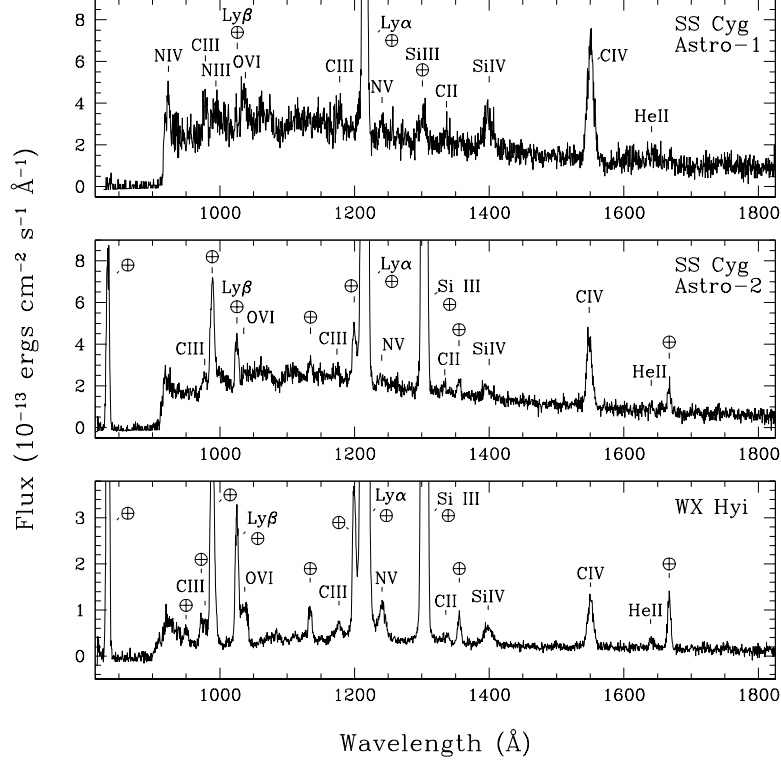


FIG. 1.— The time-averaged HUT spectra of SS Cyg and WX Hyi in quiescence. The emission lines are labelled and prominent airglow emission is marked with circled crosses.

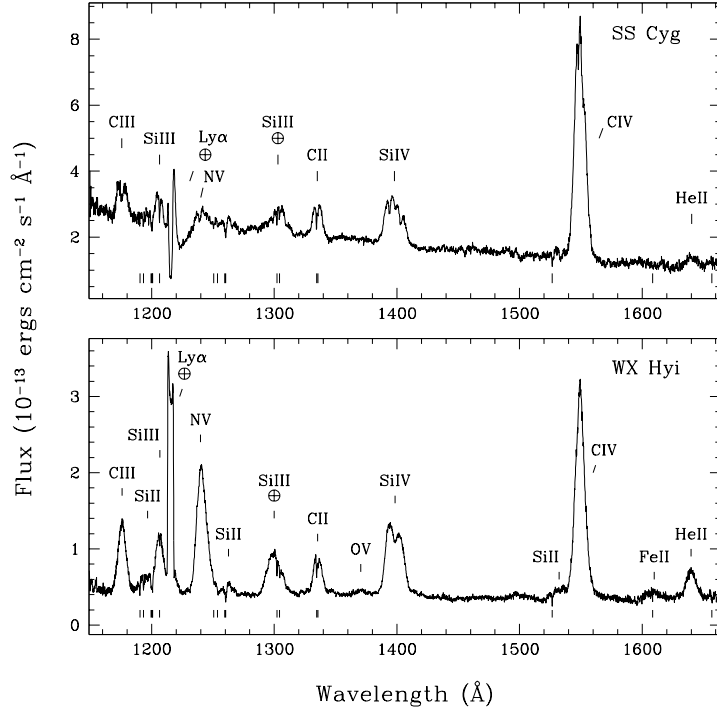


FIG. 2.— The time-averaged GHRs spectra of SS Cyg and WX Hyi in quiescence. The emission lines are labelled. The vertical lines below each spectrum indicate the location of the interstellar absorption features. Emission lines that are or may be affected by airglow are labelled with circled crosses.

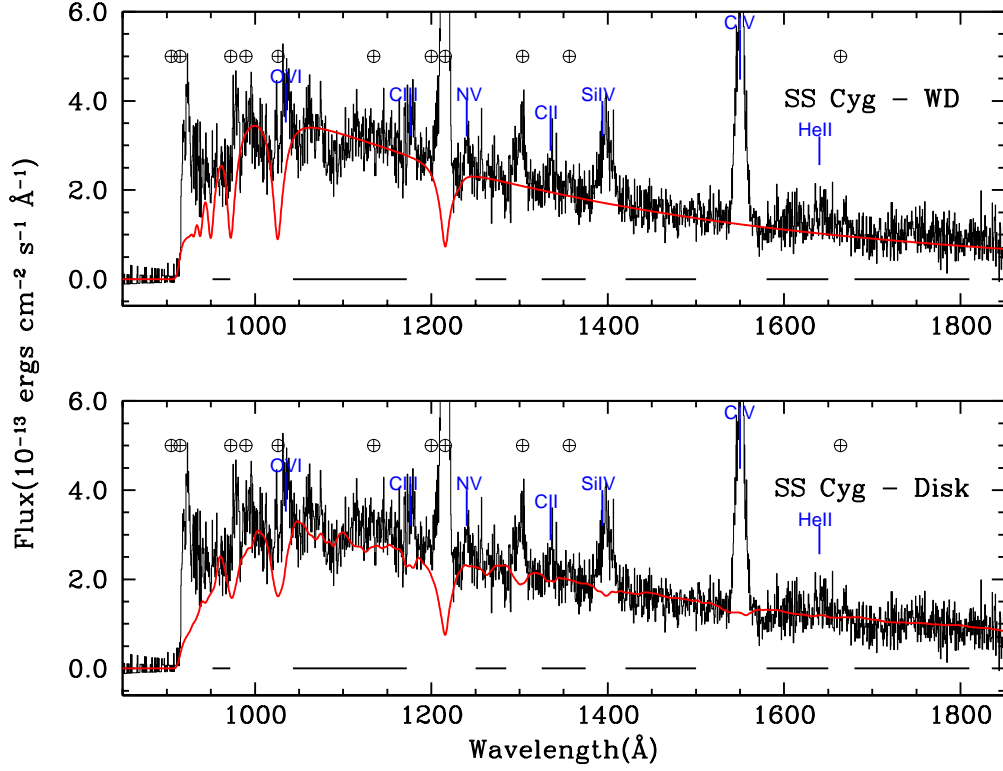


FIG. 3.— Best-fitting DA WD and accretion disk model fits to the HUT spectrum of SS Cyg. The reddening is set to  $E(B-V) = 0.04$ . The regions included in the fit are indicated by the bars under the spectra. Regions with strong source or airglow lines were excluded.

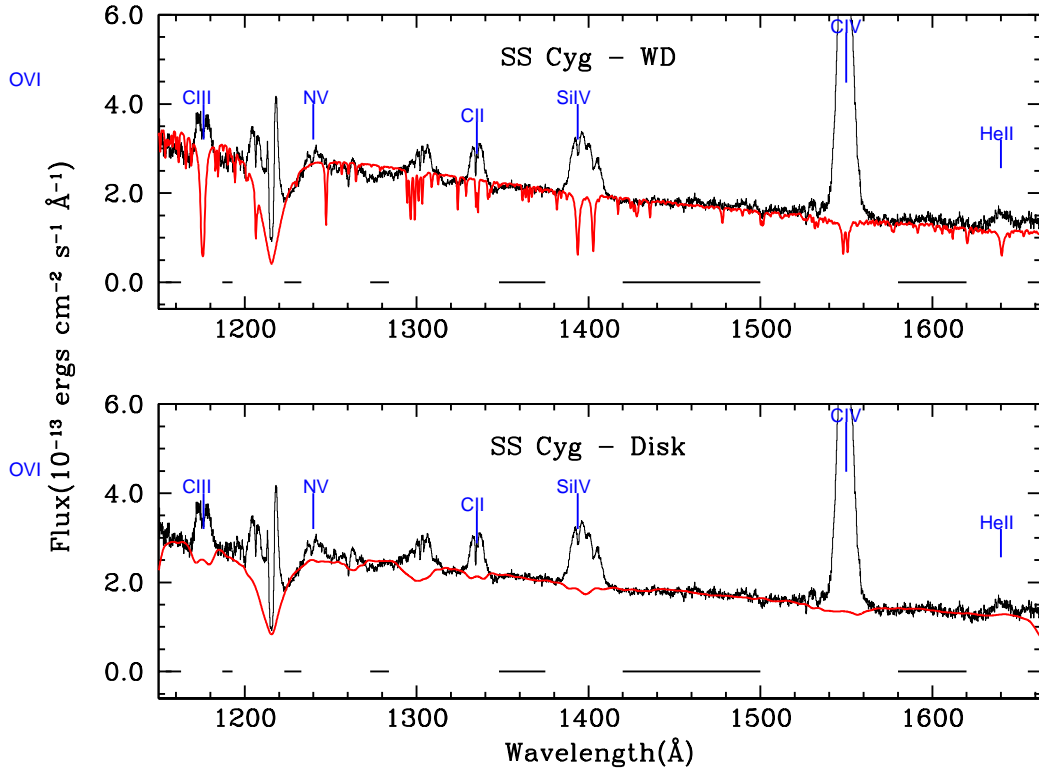


FIG. 4.— Best-fitting normal abundance WD and accretion disk model fits to the GHRs spectrum of SS Cyg. The reddening is set to  $E(B-V) = 0.04$ .

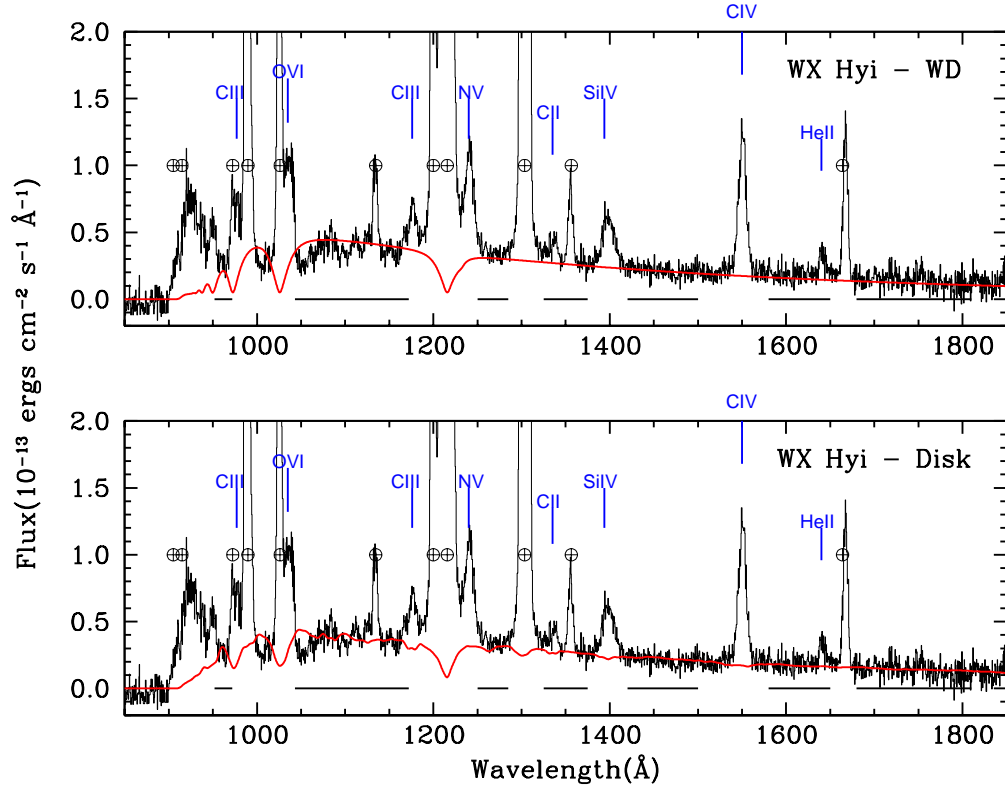


FIG. 5.— Best-fitting DA WD and accretion disk model fits to the HUT spectrum of WX Hyi.

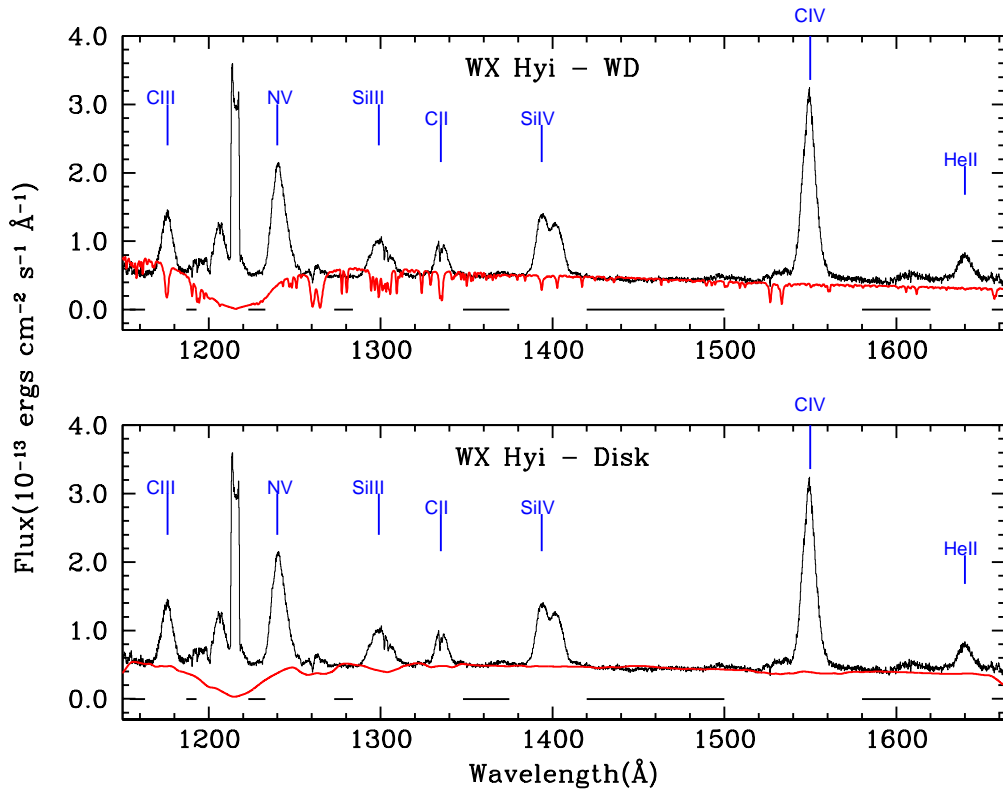


FIG. 6.— Best-fitting normal abundance WD and accretion disk model fits to the GHRs spectrum of WX Hyi.

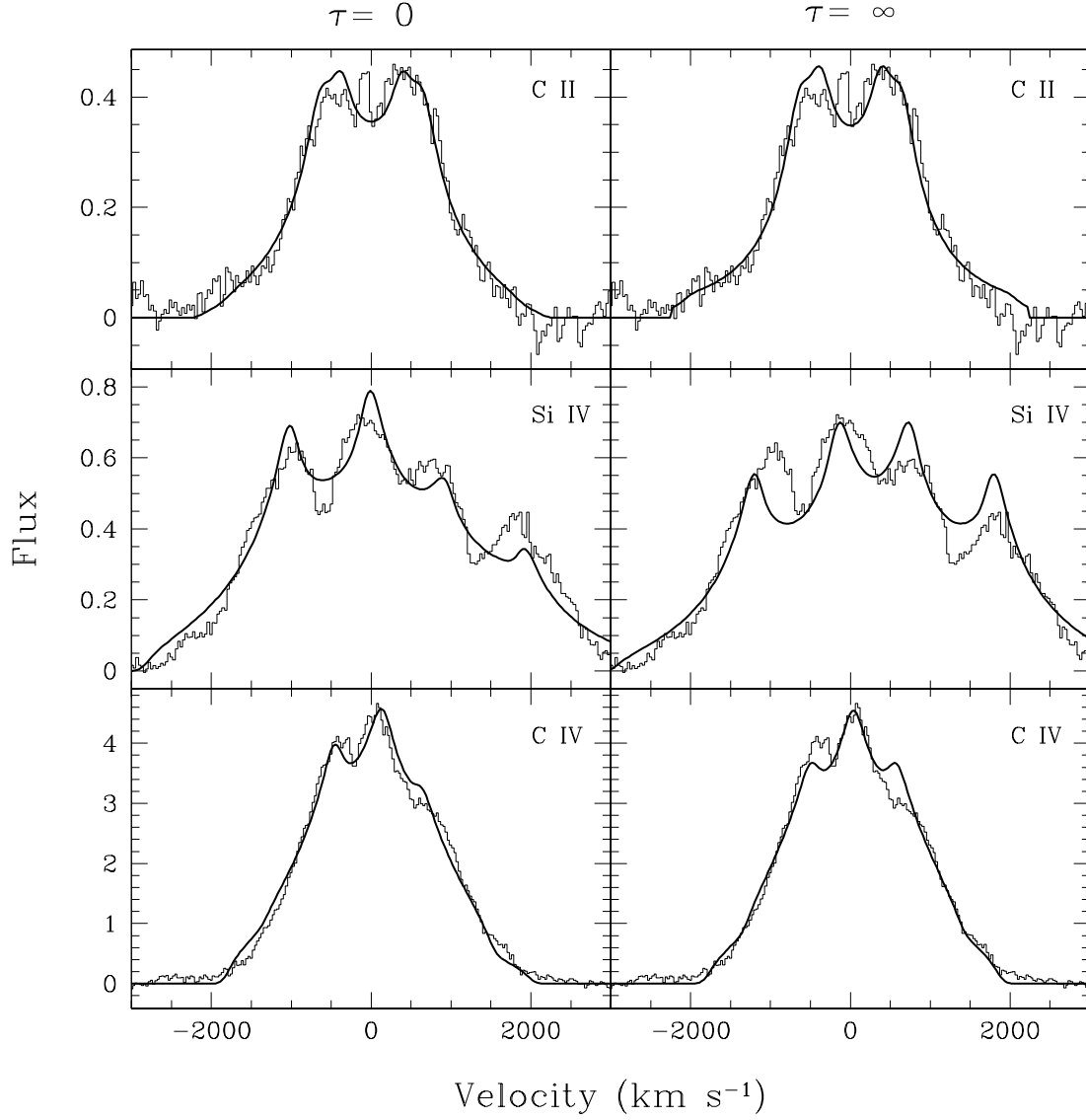


FIG. 7.— Model fits to the emission line profiles in SS Cyg. The continuum has been normalized to 1 and subtracted from the line profiles. From top to bottom, C II, Si IV, and C IV are shown. Fits in the left panels assume optically thin emission lines, while fits in the right panel are for optically thick lines. N V and He II are not fit due to the weakness of these lines.

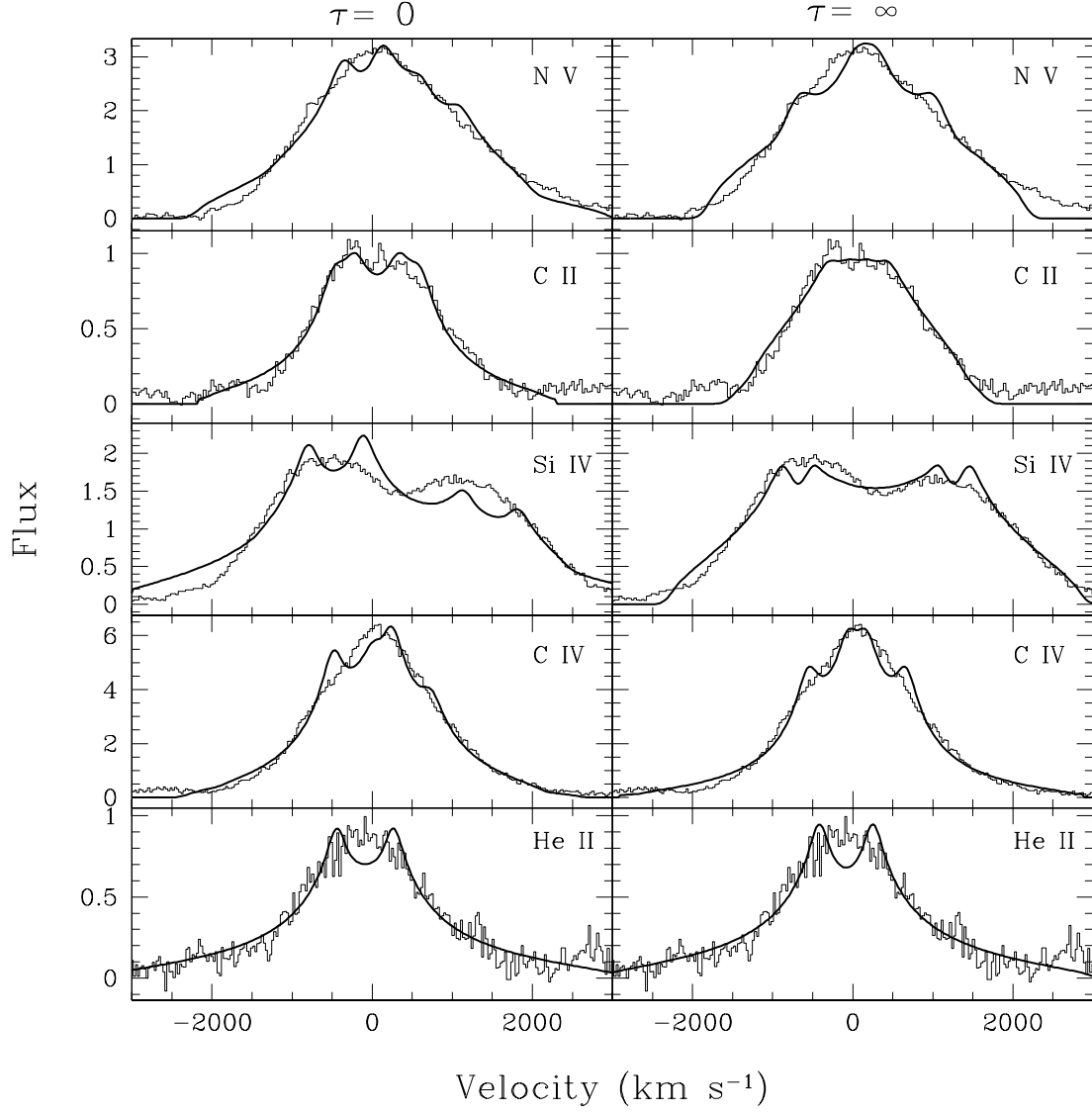


FIG. 8.— Model fits to the normalized and continuum subtracted emission line profiles in WX Hyi. N V, C II, Si IV, C IV, and He II are shown from top to bottom. The models in the left panel are for optically thin lines, while the models in the right panel are for optically thick lines.

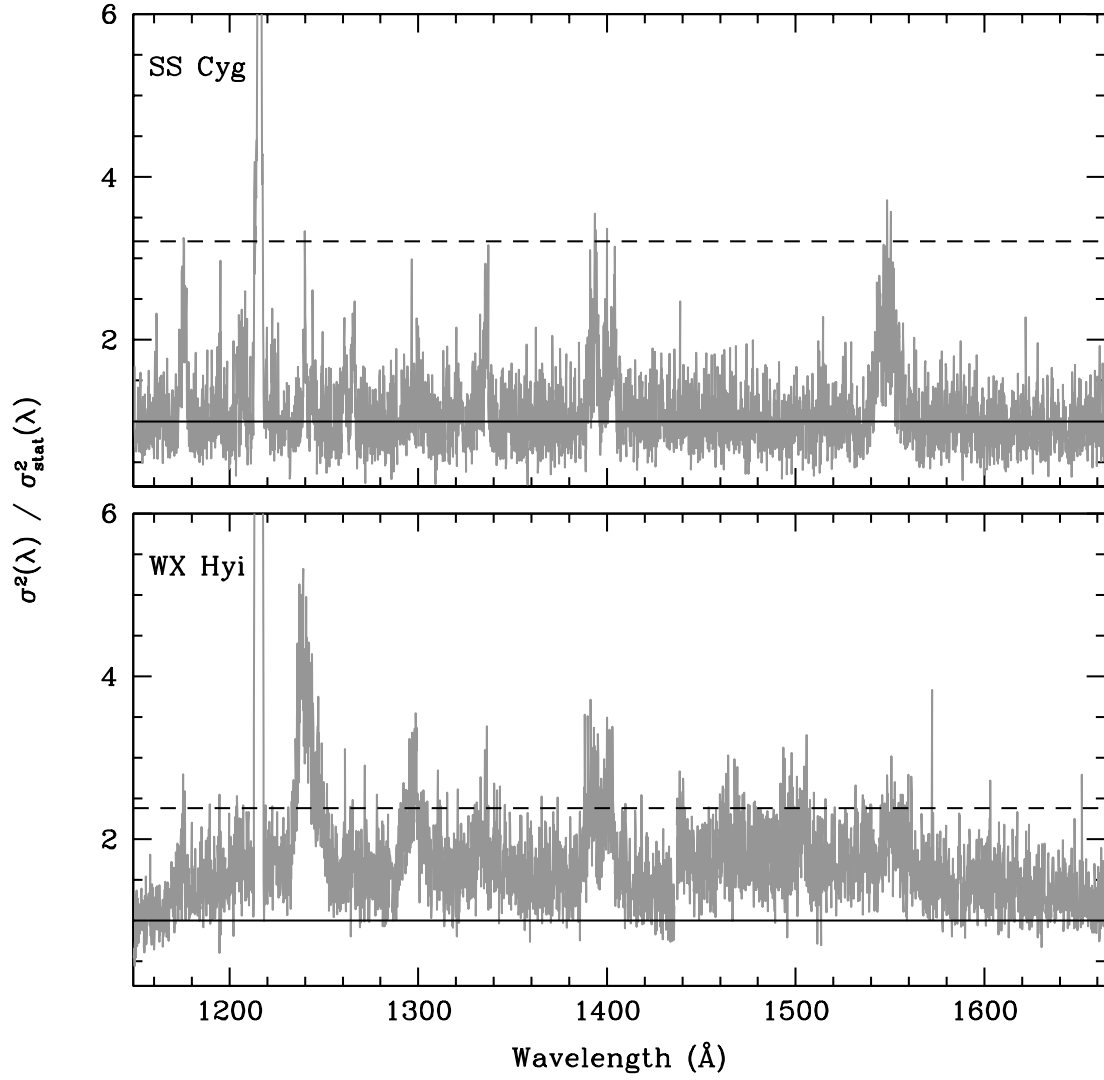


FIG. 9.— The ratio of the observed variance in the spectra of SS Cyg and WX Hyi to the variance expected from counting statistics. The solid line indicates a ratio of 1, the expectation value for no intrinsic source variability. The dashed line shows the 1% probability line for a single point exceeding this level in the case of no intrinsic variability.



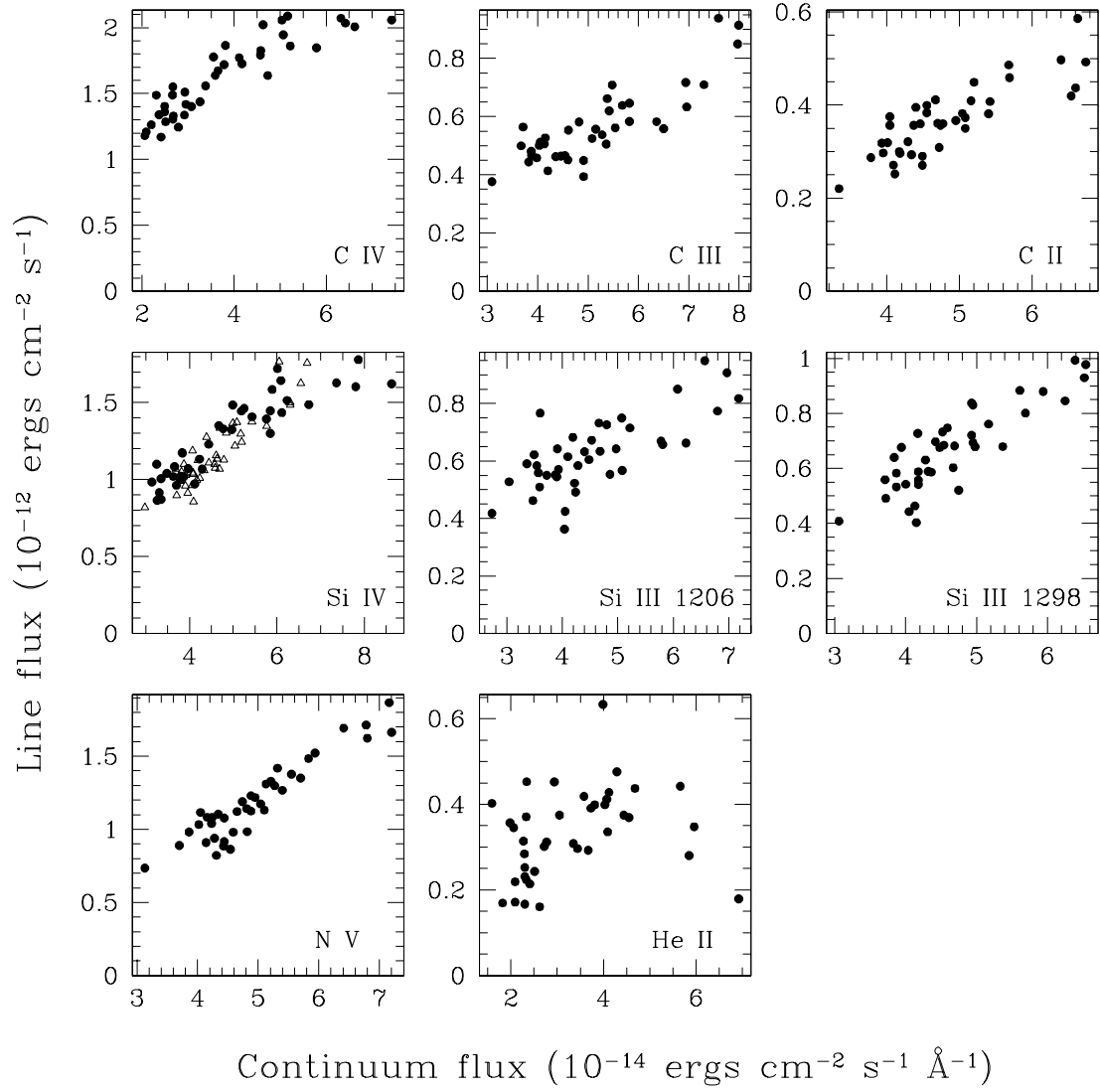


FIG. 10.— Emission line flux versus continuum flux level for the strong emission lines in WX Hyi. For Si IV, the open triangles show frames acquired in the short wavelength grating setting, while the filled circles were taken in the long wavelength setting.

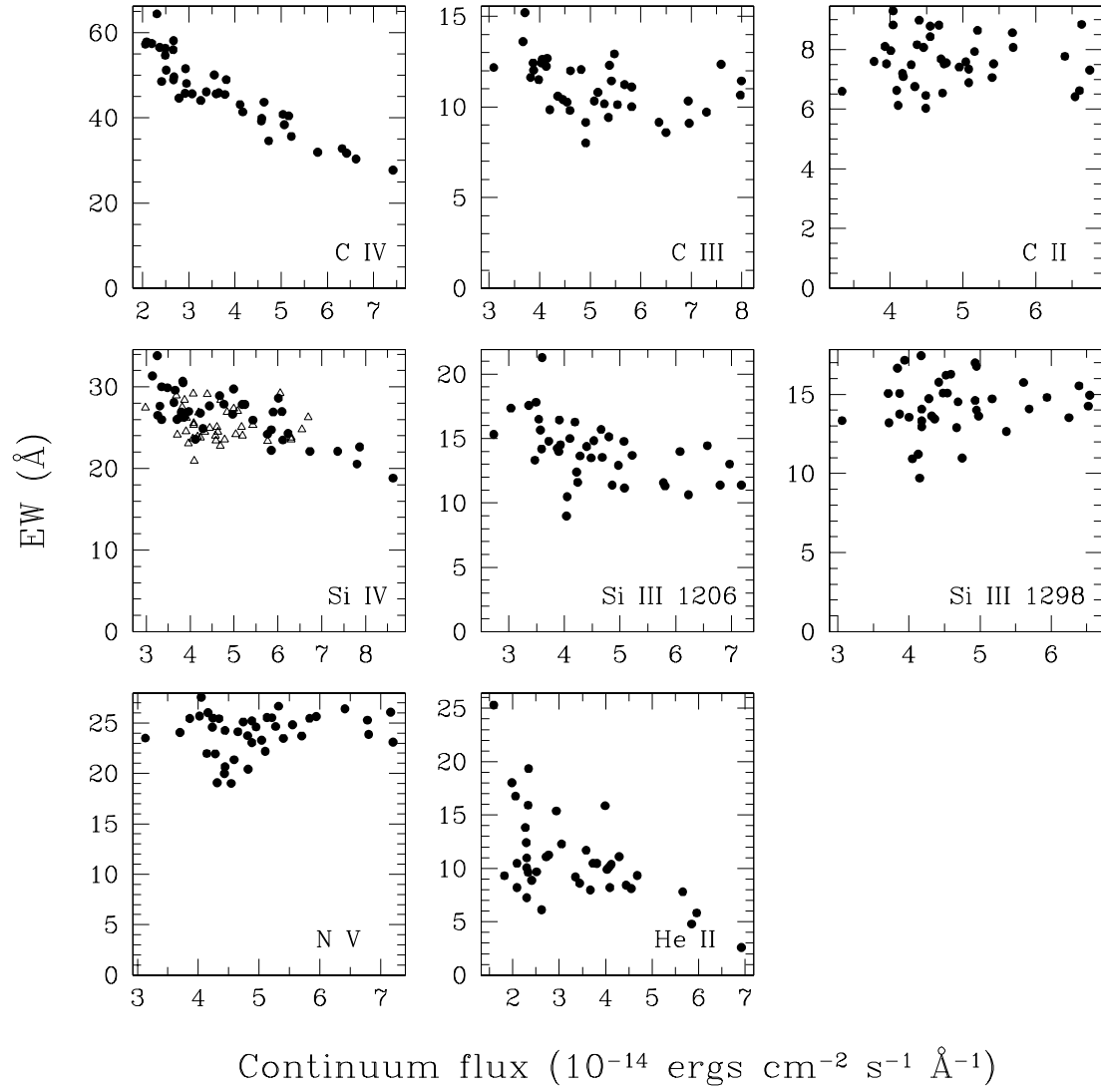


FIG. 11.— Equivalent width versus continuum flux level for the strong emission lines in WX Hyi. The open triangles and filled circles in the Si IV plot distinguish between frames taken in the shorter and longer wavelength grating settings, respectively.

TABLE 1  
OBSERVATION SUMMARY

Target	Date (UT)	Instrument	UT Start	$T_{exp}$ (s)	Wavelength Range (Å)
SS Cyg	1990 Dec 10	HUT	14:04	814 <sup>a</sup>	827 – 1878
	1995 Mar 8	HUT	17:20	320	816 – 1877
	1995 Mar 8	HUT	17:28	768	816 – 1877
	1996 Sept 26	GHRs	14:27	2176	1149 – 1436
	1996 Sept 26	GHRs	15:55	2176	1377 – 1664
WX Hyi	1995 Mar 9	HUT	02:34	1032	816 – 1877
	1995 Mar 10	HUT	13:29	1620	816 – 1877
	1995 Mar 12	HUT	05:15	1616	816 – 1877
	1996 Aug 5	GHRs	22:52	2176	1149 – 1436
	1996 Aug 6	GHRs	00:04	2176	1377 – 1663
	1996 Aug 6	GHRs	00:44	2176	1149 – 1436
	1996 Aug 6	GHRs	01:57	2176	1377 – 1663

<sup>a</sup>Portion of the spectrum obtained during the night. The total observation time was 1476 sec.

TABLE 2  
WD AND DISK MODEL FITS TO SS CYG

Model Type	Spectrum	E(B-V)	WD		Disk		$\chi^2/dof$
			Norm <sup>a</sup>	$T_{wd}$	Norm <sup>b</sup>	$\log(\dot{m})^c$	
WD(norm <sup>d</sup> )	GHRs	0.04	4.88(–23)	36,800	...	...	6218/1277
WD(DA)	GHRs	0.04	4.56(–23)	40,800	...	...	3487/1277
Disk	GHRs	0.04	...	...	0.163	16.63	2102/1277
WD(DA)+Disk	GHRs	0.04	...	...	0.171	16.66	2097/1277
WD(norm)+Disk	GHRs	0.04	0.02(–23)	58,100	0.174	16.59	2097/1277
WD(norm)	HUT	0.04	2.69(–23)	48,500	...	...	1342/1001
WD(DA)	HUT	0.04	3.26(–23)	46,000	...	...	1323/1001
Disk	HUT	0.04	...	...	0.075	17.0	1336/1001
WD(DA)+Disk	HUT	0.04	3.06(–23)	28,700	0.007	18.17	1249/1001
WD(norm)+Disk	HUT	0.04	0.89(–23)	60,000	0.136	16.31	1256/1001

<sup>a</sup>The WD model normalization  $N = 4 * \pi (R/D)^2$ , where  $R_{wd}$  is the WD radius and D is the distance.

<sup>b</sup>The disk models are normalized to a distance of 100 pc, and scale as  $D/100 \text{ pc}^2$

<sup>c</sup> $\dot{m}$  in  $g \text{ s}^{-1}$

<sup>d</sup>Normal abundance model.

TABLE 3  
WD AND DISK MODEL FITS TO WX HYI

Model Type	Spectrum	E(B-V)	WD		Disk		$\chi^2/dof$
			Norm. <sup>a</sup>	$T_{wd}$	Norm. <sup>b</sup>	$\log(\dot{m})^c$	
WD(norm <sup>d</sup> )	GHRs	0.04	5.32(–23)	24,800	...	...	3123/957
WD(DA)	GHRs	0.04	1.11(–22)	20,700	...	...	1062/957
Disk	GHRs	0.04	...	...	0.435	15.53	1286/957
WD(DA)+Disk	GHRs	0.04	1.11(–22)	20,700	...	...	1062/957
WD(norm)+Disk	GHRs	0.04	1.39(–24)	76,700	1.13	15.08	1173/957
WD(norm)	HUT	0.04	0.67(–23)	57,500	...	...	5815/989
WD(DA)	HUT	0.04	0.75(–23)	53,800	...	...	5382/989
Disk	HUT	0.04	...	...	0.011	16.71	2919/989
WD(DA)+Disk	HUT	0.04	8.41(–25)	109,000	0.141	15.50	2745/989
WD(norm)+Disk	HUT	0.04	...	...	0.06	17.02	5498/957

<sup>a</sup>The WD model normalization  $N = 4 * \pi (R/D)^2$ , where  $R_{wd}$  is the WD radius and D is the distance.

<sup>b</sup>The disk models are normalized to a distance of 100 pc, and scale as  $D/100pc^2$

<sup>c</sup> $\dot{m}$  in  $g \text{ s}^{-1}$

<sup>d</sup>Normal abundance model.

TABLE 4  
OBSERVED AND PREDICTED LINE RATIOS AND RADIAL LINE PROFILES

	N V $\lambda 1240$	C II $\lambda 1335$	Si IV $\lambda 1400$	C IV $\lambda 1550$	He II $\lambda 1640$
Line Flux Relative to C II					
SS Cyg	0.42	1.00	2.42	5.65	0.44
WX Hyi	3.32	1.00	3.19	4.59	0.86
KLSK96 Case 8 <sup>a</sup>	4.41	1.00	4.21	7.90	3.10
KLSK96 Case 9 <sup>a</sup>	1.80	1.00	2.85	5.27	2.26
KLSK96 Case 10 <sup>a</sup>	0.93	1.00	1.02	2.09	0.73
Surface brightness power law index $\alpha$					
SS Cyg ( $\tau = 0$ ) <sup>b</sup>	...	$1.77^{+0.00}_{-0.41}$	$2.07^{+0.34}_{-0.12}$	$2.35^{+0.14}_{-0.02}$	...
SS Cyg ( $\tau = \infty$ ) <sup>c</sup>	...	$1.41^{+0.24}_{-0.09}$	$2.03^{+0.58}_{-0.20}$	$2.37^{+0.06}_{-0.16}$	...
WX Hyi ( $\tau = 0$ ) <sup>b</sup>	$2.34^{+0.13}_{-0.09}$	$1.87^{+0.08}_{-0.10}$	$2.22^{+0.04}_{-0.04}$	$2.07^{+0.09}_{-0.12}$	$2.07^{+0.09}_{-0.12}$
WX Hyi ( $\tau = \infty$ ) <sup>c</sup>	$2.71^{+0.07}_{-0.37}$	$1.91^{+0.14}_{-0.10}$	$2.48^{+0.01}_{-0.03}$	$1.80^{+0.20}_{-0.10}$	$2.08^{+0.08}_{-0.11}$
KLSK96 Case 8 <sup>a</sup>	$1.14 \pm 0.05$	$1.56 \pm 0.12$	$1.16 \pm 0.05$	$0.92 \pm 0.03$	$0.93 \pm 0.03$
KLSK96 Case 9 <sup>a</sup>	$1.52 \pm 0.02$	$1.85 \pm 0.09$	$1.55 \pm 0.04$	$1.22 \pm 0.04$	$1.30 \pm 0.06$
KLSK96 Case 10 <sup>a</sup>	$1.46 \pm 0.04$	$1.36 \pm 0.07$	$1.49 \pm 0.05$	$1.22 \pm 0.01$	$1.30 \pm 0.07$
$R_{outer}/R_{inner}$ of line emitting region					
SS Cyg ( $\tau = 0$ ) <sup>b</sup>	...	$17.2^{+82.8}_{-0.67}$	$24.8^{+29.3}_{-7.90}$	$35.9^{+19.3}_{-6.7}$	...
SS Cyg ( $\tau = \infty$ ) <sup>c</sup>	...	$100.0^{+0.0}_{-81.2}$	$21.3^{+29.2}_{-4.8}$	$33.4^{+7.7}_{-8.2}$	...
WX Hyi ( $\tau = 0$ ) <sup>b</sup>	$98.6^{+1.4}_{-90.4}$	$37.6^{+23.1}_{-7.0}$	$88.0^{+12.0}_{-46.8}$	$43.1^{+56.9}_{-4.8}$	$100.0^{+0.0}_{-0.02}$
WX Hyi ( $\tau = \infty$ ) <sup>c</sup>	$24.8^{+75.2}_{-17.6}$	$40.2^{+23.4}_{-6.2}$	$100.0^{+0.0}_{-31.5}$	$73.2^{+0.0}_{-33.2}$	$100.0^{+0.01}_{-12.6}$
$V_{disk} \sin i$ (km s <sup>-1</sup> )					
SS Cyg ( $\tau = 0$ ) <sup>b</sup>	...	$490^{+75}_{-33}$	$470^{+52}_{-44}$	$280^{+19}_{-60}$	...
SS Cyg ( $\tau = \infty$ ) <sup>c</sup>	...	$520^{+34}_{-90}$	$470^{+69}_{-230}$	$280^{+62}_{-30}$	...
WX Hyi ( $\tau = 0$ ) <sup>b</sup>	$210^{+350}_{-25}$	$380^{+34}_{-37}$	$310^{+53}_{-24}$	$340^{+3}_{-180}$	$330^{+73}_{-40}$
WX Hyi ( $\tau = \infty$ ) <sup>c</sup>	$310^{+290}_{-160}$	$360^{+36}_{-52}$	$160^{+34}_{-5.1}$	$350^{+44}_{-33}$	$310^{+61}_{-43}$

<sup>a</sup> Line flux and radial line emissivity predictions from the models of Ko et al. (1996), labelled here for clarity as KLSK96. Cases 8 – 10 invoke a two-component model for the photoionizing continuum. The hard component in all three cases is a 5 keV Bremsstrahlung with  $L_X = 9 \times 10^{29}$  ergs s<sup>-1</sup>. For Case 8, the soft component is a 0.1 keV Bremsstrahlung with  $L_X = 10^{33}$  ergs s<sup>-1</sup>. For Case 9, the soft component is a 0.1 keV Bremsstrahlung with  $L_X = 10^{32}$  ergs s<sup>-1</sup>. For Case 10, the soft component is a  $5 \times 10^5$  blackbody with  $L_X = 10^{32}$  ergs s<sup>-1</sup>. The UV line flux ratios have been taken from Table 7, while the radial power law emissivity indices have been derived from the UV line fluxes in Table 4 of Ko et al. (1996).

<sup>b</sup>Power law indices for models marked  $\tau = 0$  have been derived from the observations under the assumption that the lines are optically thin.

<sup>c</sup>Power law indices for models marked  $\tau = \infty$  have been derived from the observations under the assumption that the lines are optically thick.